Antiphase dynamics and polarization effects in the Nd-doped fiber laser

S. Bielawski, D. Derozier, and P. Glorieux

Laboratoire de Spectroscopie Hertzienne, Université des Sciences et Techniques de Lille Flandres-Artois,
F-59655 Villeneuve d'Ascq CEDEX, France

The response of an Nd-doped optical fiber laser to modulation of the pump power reveals that the polarization of the laser light plays an important role in the linear and nonlinear dynamics of this laser. Experiments have been carried out under pulsed or sinusoidal modulation of the pump power as well as in the continuous-wave regime. Most of the observed phenomena may be interpreted in the framework of a theory of the two-mode laser in which each mode is associated with one polarization eigenstate of the laser. Effects such as the appearance of slow modes and antiphase behavior have also been observed. A model of a two-mode laser including spontaneous emission is theoretically and numerically analyzed. It reproduces well most of the experimental findings.

I. INTRODUCTION

In addition to their interest in connection with their application in telecommunication networks, the optical fiber lasers (OFL's) provide a rich test bench for the study of dynamics in nonlinear optical systems. Because of the broad gain profile and the long cavity length, a large number of longitudinal modes can oscillate, and these lasers are usually strongly multimode when operated well above threshold. Recent theories on modulated multimode lasers have predicted that they should exhibit a variety of dynamical effects such as antiphase dynamics and winner-takes-all motion [1], and OFL's may be used to check some predictions of these theories [2]. In a previous paper, we reported on laser dynamics monitored through the total intensity emitted by the laser [3]. Chaos following a period-doubling cascade and generalized bistability between different attractors were observed in such a laser with pump modulation. In the laser cavities with polarization-selective elements, the state of polarization of the emitted radiation is fixed by these elements. This is the case of most lasers whose instabilities have been studied up to now. On the contrary, OFL's with butt-coupled mirrors do not include such elements, and there is additional degrees of freedom due to polarization. In particular this can give rise to dynamical effects in which the polarization state of the laser light changes in addition to the amplitude or the phase instabilities that are usually investigated. Polarization eigenstates, i.e., states which replicate after a round-trip in the cavity, appear to provide the relevant basis for describing the polarization dynamics. In our OFL, they correspond to two orthogonal linear polarizations. In order to investigate how the degrees of freedom associated with polarization may influence the laser dynamics, we have carried out polarization-resolved experiments in which the laser intensities along the two polarization eigendirections are simultaneously monitored. These results are compared with the predictions of simple theoretical models for OFL's in order to find the relevant physical phenomena involved in the observed dynamics.

The consideration of laser polarization is not new and this subject has been extensively studied [4]. Since the very first days of the He-Ne laser, it was observed that alternation of orthogonal linear polarization states occurs in multimode lasers, and Zeeman lasers are known to exhibit a variety of polarization emission modes [5]. Laser emission in anisotropic crystals is also polarization dependent as shown, for instance, in the $LiNdP_4O_{12}$ laser [6]. The situation is somehow different in optical fiber lasers because the silica matrix in which the rare-earth ions are embedded is isotropic as long as its small stress-induced birefringence is neglected. In a first step this effect is considered to be small. Although spectrally equivalent sites in the silica are assumed to be isotropically distributed, the cross section for light amplification is polarization dependent. An important consequence is the phenomenon of polarization hole burning [7]. In OFL's local fields create a Stark splitting of the energy levels. Since the pump radiation is polarized, the Stark sublevels experience different pumping strength. As a consequence of different pumping and also of different emission strengths, the unsaturated gain is different for different polarization states of the field. Similar effects occur in optically pumped far-infrared lasers where the isotropy of the molecular gas is lifted by the polarized pumping field, an effect whose influence on laser dynamics was recently considered [8] and in dye lasers with fixed polarization where the gain depends on the direction of polarization [9].

This paper is organized as follows. We report in Sec. II on the static characteristics of the OFL. More specifically we show that considering the polarization of the laser radiation is necessary to understand the observed steady bifurcations. The transient response of the laser following a small perturbation of the pump is described in Sec. III and the occurrence of slow time scales is demonstrated. The nonlinear response of the laser to a strong sinusoidal modulation is studied in Sec. IV. A model is proposed in Sec. V to describe both the static

and the dynamic properties of our fiber laser. Its steady-state solutions are discussed, and a linear stability analysis is performed to check the adequacy of the model in connection with the experimental study of the transients. Numerical simulations in the strong modulation situation are required to compare the predictions of the model with the experimental findings in the strongly nonlinear case as shown in Sec. VIII. These comparisons have been carried out not only on the signal but on information more specific to nonlinear dynamics such as reconstructed attractors, Poincaré sections, and bifurcation diagrams. All these indicate that a model of two-mode laser including spontaneous emission describes the details of the OFL nonlinear dynamics.

II. POLARIZATION-RESOLVED INVESTIGATION OF THE cw CHARACTERISTICS OF THE OFL

The experimental setup, which is schematically shown in Fig. 1, is basically the same as in our previous study [3] except for the detection part which includes simple systems for polarization and wavelength analysis. The active medium of the optical fiber laser is a 5-m-long silica fiber doped with 300 ppm Nd^{3+}. The core diameter is 5.8 μm, and the fiber is single mode at the laser operating wavelength ($\lambda = 1.08$ μm), but the two linearly polarized modes LP_{01} and LP_{11} may propagate at the pump wavelength. The excitation of the LP_{11} pump mode reduces the pumping efficiency of the laser because of the poor spatial overlap between this mode and the lasing mode [10]. However, the dynamics of such a transverse single-mode laser is not expected to be qualitatively affected by the spatial structure of the pump field [11].

The laser cavity is limited by two dichroic mirrors transparent at the pump wavelength and with reflection coefficients $R_1 > 99.5\%, R_2 = 95\%$ around 1.08 μm. The former is coupled to the fiber with an index-matching liquid in order to decrease the losses, and the output mirror is simply butt-coupled to the fiber. The Fabry-Pérot effect resulting from the small gap between the fiber and output mirror allows the tuning of the laser emission
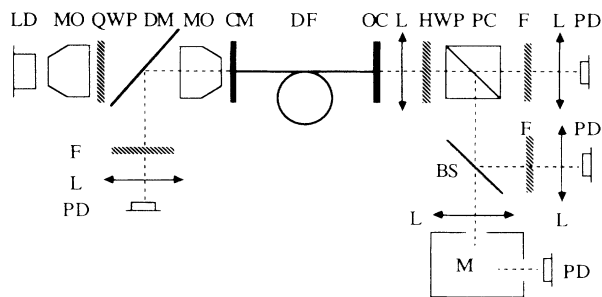

FIG. 1. Experimental arrangement for a diode pumped monomode fiber laser. Notation used: LD, laser diode; MO microscope objectives (NG 10); QWP, quarter-wave plate (820 nm); DM, dichroic mirror (R_{max} at 1080 nm, T_{max} at 820 nm); CM, coupling mirror ($R > 99.5\%$ at 1080 nm, T_{max} at 820 nm); DF, Nd-doped fiber, OC, output coupler (95%); L, lens; HWP, half-wave plate (1080 nm); PC, polarizing cube; F, bandpass filter (1060–1100 nm); BS, beam splitter; M, monochromator; PD, silicon photodiodes.

around 1.08 μm. The pump radiation, emitted at 820 nm by a polarized single-mode laser diode (RTC Philips CQL 44), is focused into the fiber through two$\times$10 microscope objectives. Between the two objectives, a quarter-wave plate allows us to vary the pump polarization, and a tilted dichroic mirror [maximum transmission (T_{max}) at 820 nm, maximum reflection (R_{max}) at 1.08 μm] is used to strongly reduce the possible feedback from the OFL power on the laser diode. The two orthogonal polarizations are separated by a polarizing beam splitter, a half-wave plate is used to select the direction of analysis. The laser intensities are monitored by silicium photodiodes with a bandpass filter ($\Delta\lambda = 50$ nm) to block the stray pump laser radiation. A beam splitter is used after the polarization selection to send a part of the laser intensity into a monochromator for spectral analysis. The rotation of the half-wave plate permits calibration of the two detectors and at the same time analysis of the spectrum on the two orthogonal polarizations.

In typical operating conditions, a pump power up to 8 mW is coupled into the fiber with an typical laser threshold of 2 mW. This allows us to reach pump parameters up to 4 (the pump parameter A is the ratio of the pump power to the threshold pump power), but the output power is limited to about 300 μW. This situation has been preferred to that in which the output power is optimized because a lower threshold is favorable for laser dynamics experiments since a wide range of pump parameters can be explored. An even wider range for A was explored in preliminary studies by using high reflectivity mirrors, of course at the expense of the output power, but this does not reveal qualitatively new phenomena. So the reflectivity value of the output mirror selected here appears as a good compromise between the extended range of parameters, and the optical output power was requested for a good signal-to-noise ratio. When the pump power is twice the threshold value (i.e., $A = 2$), the laser is strongly multimode with a wide spectrum (70 cm^{-1}) which may be tuned around 1.08 μm by adjusting the mirror positions because of Fabry-Pérot effects in small gaps between the mirrors and the fiber ends.

We have investigated the polarization characteristics of the fiber laser in the case where the spectrum is centered around 1.08 μm (the differences with our previous experiments carried out at $\lambda = 1.06$ μm will be discussed in the following sections) and more specifically their variations versus the pump power. Above a first threshold P_{th1} and up to a second value P_{th2}, the laser radiation is linearly polarized. In that range, the laser power linearly increases with the pump power, and the emitted spectrum broadens as A increases (Fig. 2). However, a weak intensity ($< 5\%$) is detected on the other polarization; it may be due to defects in the detection optics. The direction of polarization of the laser emission for pump power between P_{th1} and P_{th2} can be modified by a change of bending or twisting of the fiber. However, it appears to be independent of the polarization state of the pump. This indicates that the polarization eigendirections are imposed by the birefringence of the fiber, as expected in the case of small gain anisotropy. When the pump power is increased above P_{th2}, laser light is also emitted in the
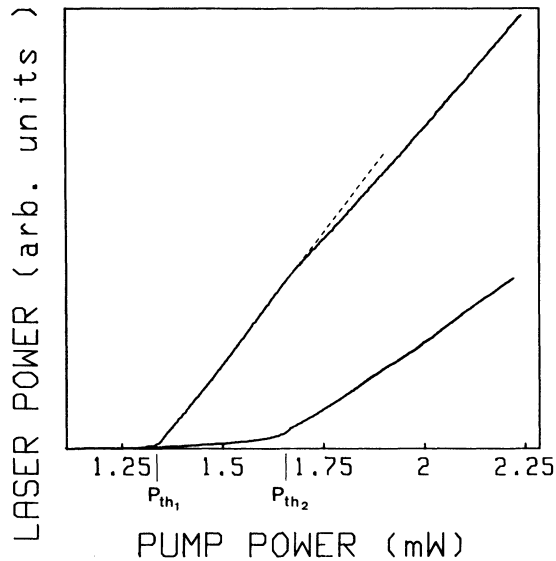
FIG. 2. cw characteristics of the OFL. Between the first and the second thresholds P_{th1} and P_{th2}, the laser emits linearly polarized radiation. Above the second threshold, it emits in both polarization directions.

polarization direction perpendicular to that observed previously. The spectral range of this emission is very narrow just after P_{th2} and it broadens as the pump power increases. Simultaneously to the appearance of this second polarization component with intensity I_2, the output power versus pump power characteristics of the first polarization component I_1 exhibits a sudden decrease of the slope (Fig. 2), but these characteristics remain linear. Above the second threshold P_{th2}, the pump power feeds two competing processes, resulting in less efficiency for the first polarization component. The value of the pump parameter at second threshold P_{th2}/P_{th1} is typically 1–1.2 and may be adjusted by acting, e.g., on the mirror position or on the fiber winding. In particular, P_{th2} can be set equal to P_{th1}, and this situation will be exploited later. The existence of two thresholds and the nature of the output versus pump power characteristics strongly suggests the existence of two competing subsystems in the fiber laser, each of these subsystems being associated with one of the two orthogonal linear polarizations.

III. POLARIZATION-RESOLVED INVESTIGATION OF THE TRANSIENT RESPONSE OF THE OFL

The fiber-laser response to a small pulse of pump power provides additional information on the physics of the fiber laser. We consider here a small step modulation of the pump parameter in a situation where the laser remains always above the first threshold P_{th1}, i.e., $A > 1$. We emphasize that this is different from the other experiments in which the pump power is on-off switched and the buildup of emission is investigated [12]. The kind of experiments carried out here can be directly compared with the results of the linear stability analysis presented in Sec. VI. For $1 \leq A \leq P_{th2}/P_{th1}$, the response to a small perturbation of the pump is a simple damped oscillation

with a single frequency, and it corresponds to the standard relaxation oscillation of a class-B laser. In our OFL, it typically occurs in the 0–20 kHz range. Hereafter, we will refer to these oscillations as "relaxation oscillations." Above the second threshold $A > P_{th2}/P_{th1}$, the laser response is made of the superposition of two damped oscillations with both different oscillation frequencies and damping coefficients. The fast one corresponds to the relaxation oscillations described above, and the slower one is associated with a new relaxation mode that appeared at the second threshold. It will be called the "low frequency" since its frequency is typically 0–0.4 times the relaxation frequency. The physical variables, i.e., the total intensity and the intensity in each polarization eigenstate are differently affected by the relaxation and the low-frequency oscillations. This is shown on Fig. 3 ($A = 2$), which displays the response of the laser in the two orthogonal polarizations corresponding to the laser eigenstates [Figs. 3(b) and (c)], together with the total intensity [Fig. 3(d)] and the pump modulation [Fig. 3(a)]. Note that the relaxation oscillations are in phase in Figs. 3(b) and 3(c). A careful examination of the corresponding signals show that their low-frequency oscillations are in opposite phase. As their amplitude is almost equal they destructively interfere in the total output intensity which displays only the high-frequency relaxation oscillations [Fig. 3(d)]. The fact that the total intensity exhibits such simple dynamics indicates that it should correspond to an eigenvector of the linear stability analysis, a result that will be checked in Sec. VI. The apparition of a slow mode and observation of a single relaxation frequency
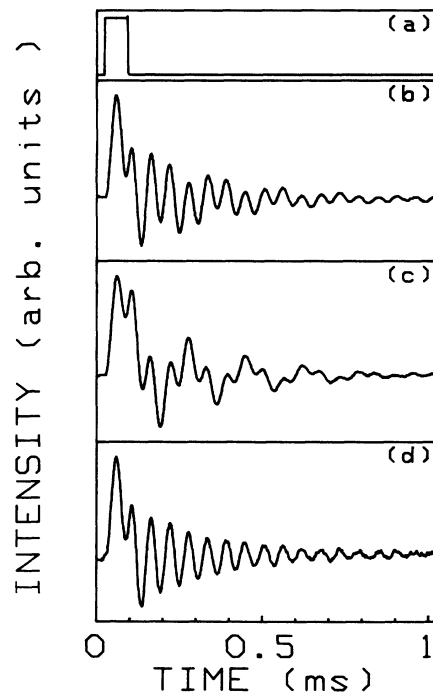

FIG. 3. Transient response of the OFL after a small perturbation of the pump intensity: (a) pump perturbation, (b) and (c) the intensities I_1 and I_2 in the two orthogonal polarization eigenstates, and (d) the total intensity.

when the total intensity is observed seem to be a general property of two-mode lasers in which the two modes are coupled via cross-saturation terms [2].

These relaxation oscillations provide us with two kinds of quantitative data: the oscillation frequencies and the damping coefficients. Their evolution versus pump power gives new information about the laser system that will give some insight on its dynamics. As mentioned in Sec. II, the laser may oscillate in the symmetric configuration in which the thresholds are the same for the two polarization states. This situation is interesting as it makes easier the comparison with the predictions of the model elaborated for the OFL since analytical calculations are readily available in the symmetric situation as shown in Sec. VI. To provide information for the comparison with theory, a series of experiments have been carried out in the symmetric situation. The corresponding measurements of the relaxation frequencies are reported on Fig. 4 together with the theoretical values from the model as given in Sec. V.

The square of the frequency of the relaxation (low-frequency) oscillations ω_r (ω_{lf}) varies linearly with the pump power (Fig. 4), as predicted by a simple rate-equation model of the two-level laser [13]. In the symmetric case studied here they both scale as $(P - P_{th})$ since both thresholds coincide. In the more general case of two different thresholds the low-frequency oscillation ω_{lf} scales as $(P - P_{th2})^{1/2}$, a general property of two-mode lasers [2]. The damping rate Γ_r of the fast relaxation oscillations strongly increases near the first threshold $A = 1$ (Fig. 4). This evolution contradicts the forecast of the simple rate-equation model mentioned above. According to this model, there is a bifurcation at the laser threshold $A = 1$ which should be accompanied by the critical slowing down as for any bifurcation. Therefore in such a model, Γ_r should tend to zero as the bifurcation at $A = 1$ is approached. In our case, the fact that Γ_r does not tend to zero implies that the threshold does not correspond to

a bifurcation. To take this into account, the model of the OFL should include terms that destroy the bifurcation at $A = 1$. As a matter of fact, if spontaneous emission is included in the equations, the total output intensity does not present any more criticality at the threshold. Spontaneous emission is known to give significant contributions to the dynamics of some guided lasers like semiconductor lasers [14] or OFL's [12], and we will show later that this effect may explain the dramatic change of the variation of the damping coefficient in the threshold region.

To summarize our conclusions from the cw and pulsed experiments, two sets of orthogonally polarized longitudinal modes appear to oscillate for different thresholds but with some similar properties. These two sets are coupled because they share at least partly the same population inversion. They relax to their steady-state through damped oscillations whose frequency is in accordance with rate-equation models but the damping divergence near threshold requires the inclusion of additional effects such as spontaneous emission.

IV. POLARIZATION-RESOLVED INVESTIGATION OF THE RESPONSE TO SINUSOIDAL MODULATION

As shown in the previous section, the transient response of the laser after a small perturbation of the pump exhibits two components with eigenfrequencies ω_r and ω_{LF}. The former corresponds to the fast-relaxation oscillation of the total laser intensity and the latter to the slow motion which is revealed by polarization-resolved experiments. These frequencies usually lie in the 15-kHz range, and modulation of the pump parameter at such frequencies is easily achieved by varying the current injected in the pump laser diode. In previous studies, the response of OFL's to sinusoidal modulation was investigated considering only the total intensity of the laser [3,15], and in Ref. [3] the laser was operated near 1.06 μm instead of 1.08 μm in the experiments reported here. We first give the results obtained at this wavelength and later discuss the differences between experiments carried out at these two wavelengths. Under high pump modulation, the laser exhibits several nonlinear effects including hysteresis and a period-doubling cascade leading to chaos, crises, generalized bistability, etc.

In this section, we investigate the correlation between the radiation emitted in the polarization states defined in the preceding section when the pump power is modulated at a frequency close to that of the fast relaxation ω_r. Figure 5 illustrates the evolution of the response of the laser on the two orthogonal polarization directions, i.e., I_1 and I_2 versus the frequency of the pump modulation. The modulation amplitude is kept constant, and the instantaneous pump power remains always above threshold. Measurements made simultaneously in the two orthogonal polarizations clearly indicate antiphase dynamics in the two polarizations. In the case of a $2T$-periodic response [Fig. 5(b)], the maximum output intensity in one polarization direction corresponds to a small peak in the other one. The same phenomenon is also observed on the
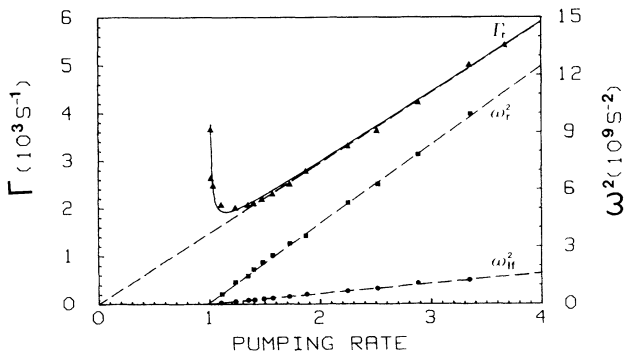

FIG. 4. Frequency and damping of the relaxation oscillations ω_r and Γ_r, and of the low-frequency oscillations ω_{lf} vs pump power. Experiments have been performed in the symmetric case. The solid line is the least-square fit of Γ_r with the real part of the eigenvalue obtained in Eq. (4). This fit leads to the determination of a (2.8×10^{-4}) and τ_f (350 μs). The dashed straight lines are the fit with $\omega_{r,lf}$ and the asymptot of Γ_r. Above threshold, this latter coincides with the curve $\Gamma_r(A)$ corresponding to $a = 0$.
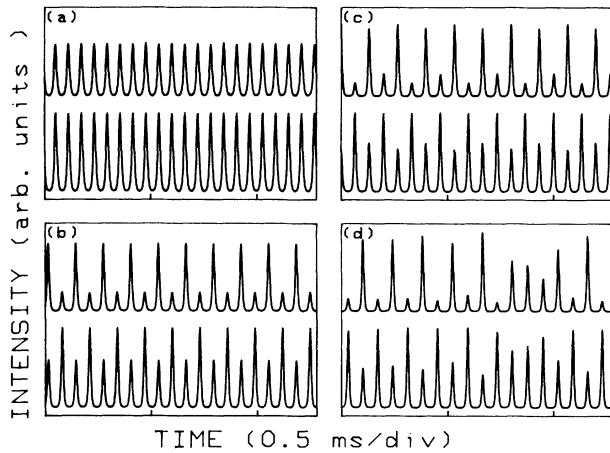
FIG. 5. Experimental evidence of antiphase response of the OFL to pump modulation in different dynamical regimes. The two series of curves are related to the intensity in each polarization eigenstate I_1 (lower traces) and I_2 (upper traces). (a) T response, (b) $2T$ response, (c) $4T$ response, (d) chaotic response.

4T-periodic signals [Fig. 5(c)] and in the chaotic regime [Fig. 5(d)]: the large peaks in one polarization are associated with small peaks in the other one. The antiphase phenomenon, which is observed between the two total output intensities in the two orthogonally polarization states, confirms the coexistence of two coupled laser systems presenting a strong competition effect. Similar antiphase motions were observed in other nonlinear systems, including lasers [1,17].

The evolution of the laser dynamics reported in the series of recordings of Fig. 5 can be summarized in a single bifurcation diagram (BD) using periodic sampling of the laser output intensity synchronously with the modulation [3]. With this technique, a sampling unit delivers a single valued output when the response of the system is T-periodic, n different values when its period is nT and scattered values for a chaotic response. BD's in the two orthogonal polarization directions do not show any significant difference in the dynamics of I_1 and I_2, supporting the fact that the two variables belong to the same dynamical system and play similar roles. Because of bistability between attractors, it is necessary to measure BD's with increasing and decreasing sweeps of the control parameter. Such a generalized bistability effect is clearly observed between 14.2 and 14.9 kHz in the case of the two BD's reported in Fig. 6. BD's obtained with the laser operating at 1.08 μm are different in two points from those reported in our previous paper, which concerns the dynamics of the OFL when the emission wavelength is centered around 1.06 μm: (i) After the crisis, the laser precipitates to a $2T$-limit cycle instead of the $4T$-limit cycle reported in Ref. [3]. (ii) The BD's at 1.08 μm appear to be more sensitive to technical fluctuations because of smaller regions of periodic behavior. For instance, the $8T$-periodic regime can hardly be seen in that case while the $16T$ regime was observed on the laser operating at 1.06 μm. The differences between the two series of BD's may be attributed to different positions of
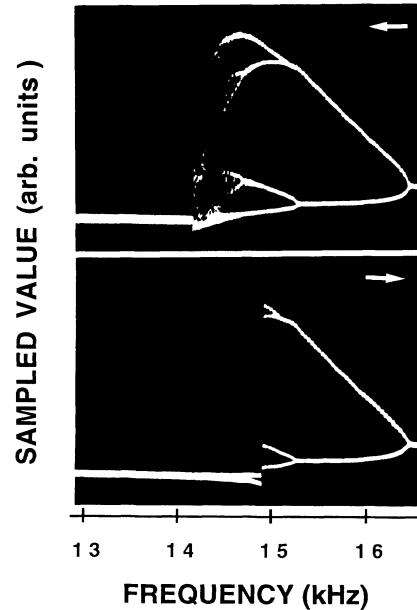

FIG. 6. Bifurcation diagram of the OFL operating at 1.08 μm. The control parameter is the frequency of the pump modulation. The upper diagram corresponds to a decreasing sweep and the lower diagram to an increasing sweep.

the laser operating wavelength in the gain profile. In this paper, the laser central frequency coincides with that of the gain line while oscillation at 1.06 μm occurs in the wing of the fluorescence spectrum, a region where the gain of the lasing modes depend strongly on their emission wavelength. They both present strong similarities with that of other nonlinear systems like the monomode CO_2 laser with modulated parameters [16]. The main difference between the OFL and the CO_2 monomode laser is that chaos appears in the OFL with a much lower modulation amplitude than predicted by the two-level model, while this model appears to describe efficiently the modulated CO_2 laser. In addition the OFL also exhibits quasiperiodicity and many more periodic windows than the CO_2 laser [16].

To investigate the chaotic regimes, the reconstruction of the attractors and Poincaré sections (or projections of these sections) have been used. Polarization-resolved experiments present the advantage of providing measurements of two dynamical variables, the intensities I_1 and I_2 in each polarization eigenstate. A projection of a Poincaré section of the attractor on a two-dimensional plane is readily obtained by combining the sampling technique with polarization resolution. An oscilloscope fed in the XY mode with the sampled values of the intensities I_1 and I_2 in the two polarization directions displays in real time a projection of a Poincaré section taken in a plane of constant phase of the modulation. The corresponding sections at different points of the inverse cascade $C2$ [18], and in the fully chaotic regime near the $2C$-C transition and just before the boundary crisis are shown on Figs. 7(a), 7(b), and 7(c), respectively. As expected, the Poincaré sections for the $C2$ regimes appear as two clusters of dots periodically visited while they span a wide region of
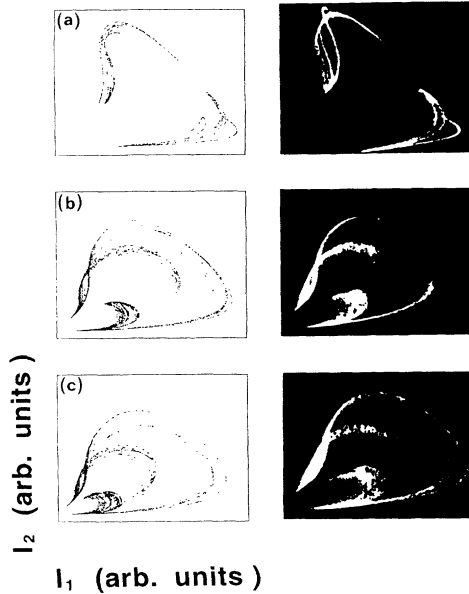
FIG. 7. Poincaré sections in chaotic regimes corresponding to different points of the inverse cascade. (a) $C2$; (b) and (c) fully chaotic regimes just after the $2C$-C transition and just before the boundary crisis. The right (left) column reports the experimental (numerical) results.

the plane beyond the end of the inverse cascade. These Poincaré sections have special shapes, they are given as a fingerprint of the chaotic attractor to be compared with the corresponding curves given by numerical simulations in the next section.

V. MODELING OF THE OFL

The strong multimode nature of the emission together with the large number of transitions that are involved in the laser operation and thus the great number of dynamical variables and laser parameters make the theoretical approach of the OFL's dynamics very difficult. Up to now, most of the models have been designed in order to understand the behavior of the OFL in the cw regime and to optimize the performances of this kind of laser. These models are based on the rate-equation approximation and allow us to study in particular the importance of the spatial effects (mode overlap) [10], the output saturation [19], and the problems due to excited-state absorption [20].

A comparison of model predictions with the observed experimental behavior of an OFL was first performed by Hanna et al. [15]. They showed a good description of the dependence of the relaxation frequency versus the pump power in the framework of the monomode two-level class-B model. More recently, Le Flohic et al. [12] studied the transient buildup of emission in the Nd^{3+} OFL and compared their results to a two-level multimode class-B model including amplified spontaneous emission.

Despite the strongly multimode nature of the laser emission, the experimental results reported in the above sections suggest that our OFL behaves essentially as a two-mode laser in which each mode is associated with a polarization eigenstate. Therefore, we will not consider the many longitudinal modes but rather consider the

laser as made up of two subsets corresponding to two clusters of longitudinal modes, one in each of the polarization eigenstates.

Because of the short relaxation time of the coherences compared to the photon lifetime and the relaxation times of the levels involved in the lasing action, the atomic polarizations may be adiabatically eliminated, and we consider rate equations as in the models of OFL's proposed previously. All the deexcitation times except the lifetime of the upper level of the lasing transition are extremely short compared to the photon lifetime. Therefore, the only populations involved in the laser dynamics are those of the upper level of the laser transition and of the fundamental level. Moreover, the latter can be considered to be almost constant because the available pump power does not produce any bleaching at the pump wavelength.

To summarize, time scale and experimental reasons lead us to set a model of the OFL in which the laser is composed of two laser subsystems associated with the two clusters of modes in each polarization eigenstate. Each subsystem is described by a class-B model with two dynamical variables, namely its intensity and population inversion. Let us discuss now the different terms included in this model.

Spontaneous emission should be taken into account to describe correctly the variation of the damping of the relaxation oscillations Γ_r in the near-threshold region as discussed in Sec. III. This makes sense since the photons emitted by spontaneous emission have a significant probability to be trapped in the LP_{01} mode because of the wide numerical aperture of the fiber. Therefore, a non-negligible part of these photons is injected in the lasing modes and contributes to the laser dynamics. This effect is also typical of other guided lasers like the semiconductor lasers [14].

The pumping terms may be either equal or different for the two polarizations. To check the pumping anisotropy, we have realized a series of experiments in which the pump polarization is rotated. The polarization eigenstates of the laser remain the same in accordance with our interpretation according to which they are determined by the residual birefringence of the cavity. In opposition the intensity sharing between the two states of polarization changes. This polarization-selective gain occurs because both the interactions between the polarized pump and the ions, and that between the ions and the fields along each direction of polarization depend on the local field experienced by the ions. Therefore, the pumping terms corresponding to the two laser subsystems need to be taken differently in the model.

The losses are taken equal for the both linear polarizations. The bending losses give the most important contribution to the loss anisotropy since the coupling losses between the fiber and the mirrors can be considered to be isotropic. However, such bending losses are very small in our case. Therefore, we consider that all the anisotropies are taken into account by the pumping asymmetry introduced in the model. The two systems are coupled by two kinds of terms, first, a cross gain effect: The intensity of mode 1 (mode 2) is amplified by its corresponding population inversion d_1 (d_2) but also to a smaller amount by the

population inversion of the other mode d_2 (d_1). Second, the stimulated emission causes a saturation of each population by its corresponding intensity (self-saturation), but also by the other intensity (cross-saturation). The two cross-saturation coupling coefficients are taken equal. The equations of such a laser can be written in the following adimensional form:

$$\dot{m}_i = (d_i + \beta d_j - 1)m_i + a(d_i + \beta d_j) \ ,$$

$$\dot{d}_i = \gamma[d_i^0(\tau) - (1 + m_i + \beta m_j)d_i] \tag{1}$$

with $i = 1$ or 2 and $j = 3 - i$. m_i and d_i are the reduced intensities and population inversions of the two laser systems. The dots represent the derivatives with respect to a reduced time $\tau = t/\tau_c$, and τ_c is the photon lifetime in the cavity.

$d_i^0(\tau)$ are the pumping term of the two laser subsystems. $d_i^0(\tau) = d_i^0(1 + r\cos\Omega\tau)$ if the pump amplitude is sinusoidally modulated. The experimental situation corresponds to a fixed value of $\alpha = d_2^0/d_1^0$ determining the asymmetry of the system as discussed above. Without loss of generality, we assume that $\alpha \leq 1$.

$\gamma = (\tau_c/\tau_f)$ with τ_f the population inversion relaxation time. Spontaneous emission is considered through the coefficient a, which includes the spontaneous-emission probability and the waveguiding effect. β is the cross-saturation coefficient describing how each laser field is coupled with the population inversion of the other laser system. For the sake of simplicity, the cross coupling is considered to be the same for spontaneous and stimulated emissions.

This phenomenological model shares many common points with those of coupled lasers [1,2] and simple models of multimode class-B lasers [6,12,21]. We must also note that the behavior observed experimentally is also typical of two-mode lasers described by more complete models of multimode lasers including spatial hole burning [22], but we prefer here to choose a phenomenological model containing a minimum number of dynamical variables (four) and of adjustable parameters of the laser $(\alpha, \beta, \gamma, a)$.

The asymmetric case, which is the general situation for our OFL leads to much more complicated analytical results. In the Appendix we consider the asymmetric model in absence of spontaneous emission. In that situation analytical results may be obtained assuming that the inversion population lifetime is much longer than the photon lifetime $(\gamma \ll 1)$. A linear stability analysis of the steady-state solutions expanded in power series of $\gamma^{1/2}$ can be carried out under these approximations.

VI. MODELING THE OFL: SYMMETRIC CASE INCLUDING SPONTANEOUS EMISSION

We will concentrate here on the case of the symmetric laser $(\alpha = 1)$ in which both polarization eigenstates have the same unsaturated gain, a situation that can easily be reached experimentally as mentioned in Secs. II and III. In this case, the steady-state solution of the above equations can easily be found and a linear stability analysis be performed. The values derived from this analysis provide information on the response of the OFL to pulse excita-

tion and these predictions will be ultimately checked against experiments.

The symmetry of the system suggests definition of the following change of variables:

$$M = (1 + \beta)\frac{(m_1 + m_2)}{2} \ ,$$

$$\mu = (1 + \beta)\frac{(m_1 - m_2)}{2} \ ,$$

$$D = (1 + \beta)\frac{(d_1 + d_2)}{2} \ , \tag{2}$$

$$\delta = (1 + \beta)\frac{(d_1 - d_2)}{2} \ .$$

The steady-state values M_s, D_s, μ_s, δ_s of M, D, μ, δ are obtained by the resolution of $(\dot{M} = 0, \dot{D} = 0, \dot{\mu} = 0, \dot{\delta} = 0)$. The only steady state that is physically acceptable (i.e., with $M_s > 0$) is

$$M_s = \frac{1}{2}[A - 1 + \sqrt{(A - 1)^2 + 4A\epsilon}] \ ,$$

$$D_s = 1 - \frac{1}{2(1 - \epsilon)}[-(A - 1 + 2\epsilon) \\ + \sqrt{(A - 1)^2 + 4A\epsilon}] \ , \tag{3}$$

$$\mu_s = 0, \quad \delta_s = 0 \ ,$$

where $\epsilon = (1 + \beta)a$ and $A = (1 + \beta)d_1^0$ is the pump parameter, i.e., the ratio of the pump parameter to its threshold value.

Because of spontaneous emission, there is no clear discontinuity between the lasing and nonlasing regimes. In other words, the threshold of the laser does not correspond anymore to a real bifurcation but rather to an imperfect bifurcation [23].

The linear stability analysis in the symmetric case shows that the steady state is always stable. The nature of the eigenvalues depends on the pump parameter. Below a threshold approximately equal to $A = 1$ if ϵ and γ are small, the four eigenvalues are real and negative. Above this threshold, the eigenvalues are complex and have the same real parts

$$\Lambda_{\pm} = -\frac{1}{2}[1 - D_s + \gamma(1 + M_s)] \\ \pm i\{\gamma[D_s(M_s + \epsilon) + (1 - D_s)(1 + M_s)] \\ - [1 - D_s + \gamma(1 + M_s)]^2/4\}^{1/2} \ , \tag{4}$$

$$\lambda_{\pm} = -\frac{1}{2}[1 - D_s + \gamma(1 + M_s)] \\ \pm i\{\gamma[c^2 D_s(M_s + \epsilon) + (1 - D_s)(1 + M_s)] \\ - [1 - D_s + \gamma(1 + M_s)]^2/4\}^{1/2} \tag{5}$$

where $c = 1 - \beta/1 + \beta$. Far from threshold $(A \gg 1$ and $\gamma, a \ll 1)$, the imaginary parts of Λ_+ and λ_+ can be approximated as $\omega_r = \sqrt{\gamma(A - 1)}$ and $\omega_{lf} = c\omega_r$, respectively.

The corresponding eigenvectors are in the plane $(\mu = 0; \delta = 0)$ for $\Lambda_{\pm}$ and in the plane $(M = 0; D = 0)$ for $\lambda_{\pm}$. Therefore the oscillations observed in the two intensities m_1, m_2 following a small perturbation will be in

phase (antiphase) for the high (low) frequency. In the case where only the total intensity M is observed, the low frequency is perfectly masked. Moreover, the dependence of M_s, the observed relaxation frequency, and the corresponding decay with A agrees with the predictions of a two-level monomode model with spontaneous emission. This symmetry of the eigenvectors leads to a peculiar phenomenon: A small perturbation of the pump power can only excite symmetric states which keep their symmetry during their relaxation to the equilibrium. To reach asymmetric states, one needs a strong excitation such as that which would bring the system in the $2T$ regime where antiphase motion is observed. Then the antisymmetric component of the state vector is excited and therefore can be observed. This is illustrated on Fig. 8 which displays the response of the OFL to a small excitation leading to a symmetric state 8(b) and to a strong excitation in which the laser is temporarily sent onto the $2T$-periodic cycle 8(c), where as discussed in Sec. IV asymmetric motion is excited.

The model proposed here predicts the antiphase phenomenon and the increase of Γ_r when A approaches the threshold in qualitative agreement with the experimental observation. A value of a may be deduced from the fit between the experimental and theoretical values of the damping constant of the fast relaxation oscillations.

VII. MODELING THE OFL: ASYMMETRIC CASE INCLUDING SPONTANEOUS EMISSION

As in Sec. VI for any value of d_1^0 only one physically acceptable solution of (1) exists. Far from the two thresholds, the stationary solutions are close to the stable solutions of the model without spontaneous emission (as defined in the Appendix). In our case, a is smaller than γ. Then we can write $a = \eta\gamma$ and expand the steady states and their eigenvalues in a power series of $\gamma^{1/2}$ in
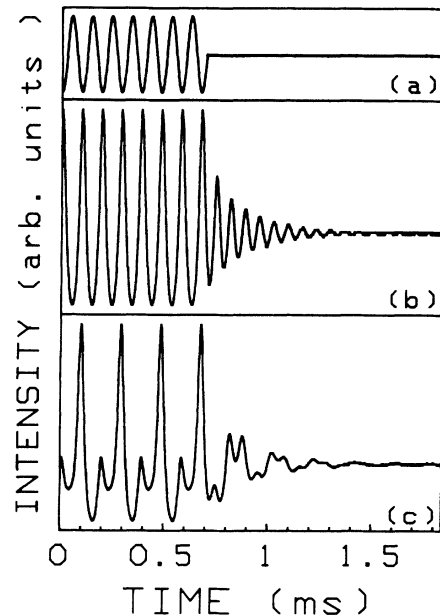

FIG. 8. Transient response of the laser in the symmetric case. (a) Pump power, (b) response of the laser after a sinusoidal modulation leading the system in a symmetric state, (c) after a modulation leading the system to a $2T$-limit cycle. The intensity is detected along one polarization eigendirection.

order to analyze the asymptotic behavior of the eigenvalues when the laser is far from threshold. The spontaneous-emission term a is found to have no effect at the first order on the values of the resonance frequencies and it only decreases the real part of the eigenvalues. In particular, the real part of the eigenvalues corresponding to the case where the pump is well above the threshold for two-mode operation is

$$\mathrm{Re}(\lambda_{1,2}) = \mathrm{Re}[\lambda_{1,2}(a=0)] - \left[\left[\frac{1}{m_1^{(0)}} + \frac{1}{m_2^{(0)}} \right] \pm \frac{1-\beta}{S}(m_1^{(0)} - m_2^{(0)}) \left[\frac{1}{m_1^{(0)}} - \frac{1}{m_2^{(0)}} \right] \right] \frac{\eta\gamma}{4} + O(\gamma^{4/2}) \qquad (6)$$

with $\mathrm{Re}[\lambda_{1,2}(a=0)]$ and $m_i^{(0)}$ the real parts of the four complex conjugate eigenvalues and the steady-state values of m_i corresponding to the case $(a=0)$ as derived in the Appendix and

$$S = \left[(m_1^{(0)} - m_2^{(0)})^2 + \frac{16\beta^2 m_1^{(0)} m_2^{(0)}}{(1+\beta)^2} \right]^{1/2} . \qquad (7)$$

We must remark that according to the predictions of the model discussed here the effect of the spontaneous emission on the steady states is too small to explain the curvatures of the output power versus pump power characteristics that have been observed experimentally near the thresholds. This could be attributed to amplified spontaneous emission in nonlasing modes as discussed by Le Flohic et al. [12]. In this transition region, the number of emitted modes rapidly and continuously increases with the pump power resulting in a smooth evolution of

the laser power near the threshold. This broadening of the emitted spectrum is very clear when the laser power is analyzed by a monochromator and its connection to laser nonlinear dynamics is being considered.

The parameters of the model corresponding to the experimental situation have been determined from the results obtained in the linear regimes. Above the second threshold, the two resonance frequencies ω_r and ω_{LF} and their associated decays have been measured for different pump powers. The variations of the eigenvalues of the model versus the pump power have been fitted with the experimental results in order to evaluate the parameters α, β, and γ. Typical orders of magnitude are $\alpha = 0.85-1$, $\beta = 0.42-0.45$, $\gamma = \tau_f/\tau_c$ depends on the cavity losses and therefore varies in a wide range, in the experimental situation of Sec. IV it is equal to 0.67×10^{-3}. These fits lead also to estimation of the upper level relaxation time τ_f. We have obtained lifetimes of 350 to 420 μs close to

the actual value (460 μs in Ref. [24]). Therefore we can consider that the model introduced here is able to describe precisely the linear dynamics of the OFL. The case of strong modulation cannot be treated analytically, and we have proceeded to numerical simulations to investigate to what extent the model is able to describe the OFL in such conditions.

VIII. NUMERICAL SIMULATIONS IN THE NONLINEAR REGIME

The numerical integration of the model equations has been carried out for different values of the parameters. We have found a good agreement between the model and the experiment if we choose parameters close to the values determined from the fits of the quantities obtained in the linear regime. For all the results presented in this section, we have taken $A = 2.8$, $r = 0.16$, $\alpha = 0.86$, $\beta = 0.43$, and $a = 1.8 \times 10^{-4}$ while the values determined from the pump diode intensity would give $A = 2.6$, $r = 0.16$ and values of α, β, and a are 0.86, 0.43 and 2.8×10^{-4}, respectively. The value of γ is 0.67×10^{-3} as discussed above.

The calculated variations of the intensities display the same spiking behavior and antiphase phenomena (Fig. 9) as the experimental signals, and chaos occurs with modulation amplitudes comparable with the experimental values. The bifurcation diagrams obtained with a sweep of the modulation frequency show the same shape as the experimental diagrams as illustrated on Fig. 10. In particular, the transition to chaos occurs after a period-doubling sequence at the high frequencies and disappears at the low frequency through a boundary crisis in which the chaotic attractor is replaced by a $2T$-limit cycle. The characterization of the chaotic attractors by the use of Poincaré sections has been carried out for different regimes of the inverse cascade. The comparison of the Poincaré sections obtained experimentally with those given by numerical simulations shows that even the detailed structure of the reconstructed attractors (Fig. 7) is the same.

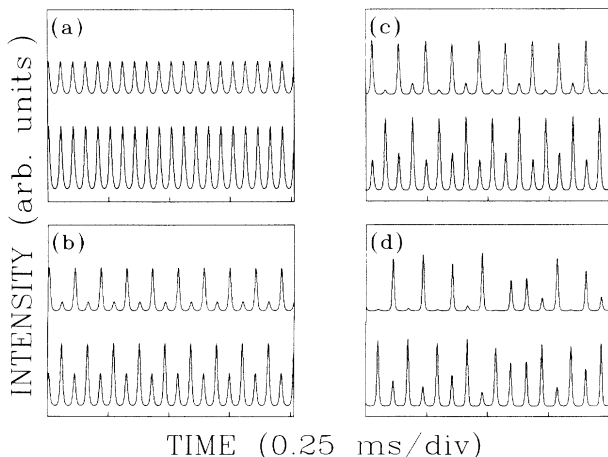The value of A and a have been adjusted to values slightly different from those calculated from the experi-

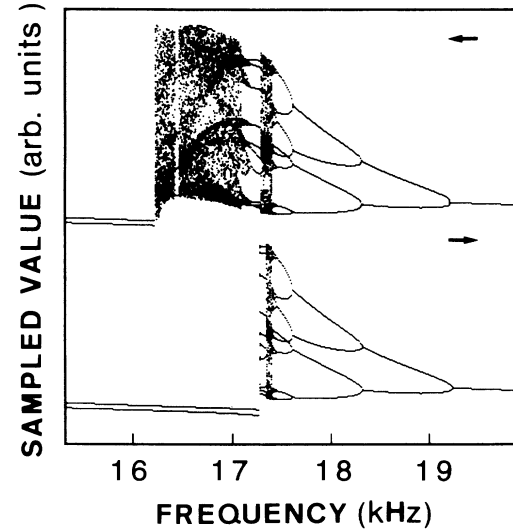

FIG. 10. Calculated bifurcation diagrams corresponding to the experimental results of Fig. 6 with $1/(\tau_c \tau_f) = 8.75 \times 10^9$ s^{-2}.

mental parameters. They were chosen because they lead to the best agreement between numerical simulations and experimental results. These small discrepancies reveal the limits of the model due to the strong simplifications introduced. In particular, the effects of the multimode nature of the field have been neglected. Moreover, the population inversion has simply been shared into two subsets although the interaction of two polarized modes implies rather complicated effects of cross saturation via spatial hole burning and polarization hole burning.

However, the smallness of the discrepancies between the results of the model and the experiments is somewhat surprising because of the apparent complexity of this strongly multimode laser. This result shows that only a few physical properties of the OFL are important in governing its dynamics. The reason for which each cluster acts as one mode is not yet well understood and deserves further investigation. This collective behavior may be due to the difference between the interaction of longitudinal modes of the same polarization and the interaction of two modes of different polarizations. A possible relevant difference is the difference of cross-saturation parameters. Indeed, the cross saturation between two longitudinal modes of the same polarization arises from spatial (and spectral) hole burning, whereas the cross saturation between two modes of different polarizations involves, in addition, polarization hole burning. Higher-order nonlinear interactions may also be involved in the collective behavior. Further experiments and models are needed in order to show up the physical origin of this "clustering" behavior. In particular, wavelength-resolved experiments are needed to know if all the modes of each cluster are actually locked together, or if some internal dynamics exists but is masked when the total intensity of each polarization is observed.

IX. CONCLUSION

The OFL under pump modulation displays an interesting variety of dynamical behavior. However the only ob-

FIG. 9. Results of the numerical simulations corresponding to Fig. 5.

servation of the total intensity emitted by the laser restricted the available insight. For instance, the antiphase motion of orthogonal polarization components was masked and the amplitude of some other effects was severely limited. Resolving the polarization state of the emitted radiation enlarged the point of view, it also allowed the easy simultaneous observation of two dynamical variables. Access to two dynamical variables also makes easier the reconstruction of the attractor and provides more significant Poincaré sections and return maps.

The measurement of the damping constants of the relaxation oscillations indicates that contrary to what occurs in most other lasers studied up to now, spontaneous emission significantly contributes to the OFL dynamics. A model for this kind of laser taking both spontaneous emission and polarization effects into account has been introduced. It reproduces well most of the experimental findings with semiempirical parameters deduced from independent experiments. In particular the agreement between the reconstructed attractors and their numerical counterparts is excellent. It should be stressed that this was obtained in spite of the drastic approximations which have been introduced in this model. For instance, the restriction of a multimode laser to a two-mode system leads to some discrepancies when a quantitative prediction is aimed, but this can be corrected by including suitably corrected parameters. The quality of the agreement on, e.g., the details of the structure of the chaotic attractors indicates that the proposed model catches the key ingredients of the OFL dynamics.

ACKNOWLEDGMENTS

APPENDIX: INVESTIGATION OF THE MODEL WITHOUT SPONTANEOUS EMISSION

The steady-state values $m_i^{(0)}$ and $d_i^{(0)}$ of m_i and d_i corresponding to the case without spontaneous emission (i.e., $a = 0$) are derived from the resolution of (1) with $\dot{m}_i = 0$, $\dot{d}_i = 0$. Three kinds of solutions are obtained.

(1) The trivial solution $m_i^{(0)} = 0$, $d_i^{(0)} = d_i^0$.

(2) The single-mode solutions

$$m_1^{(0)} = \frac{1}{2\beta} \{ \beta(d_1^0 + d_2^0) - (1+\beta)$$
$$+ ([\beta(d_1^0 + d_2^0) - (1-\beta)]^2$$
$$+ 4\beta(d_1^0 + \beta d_2^0 - 1))^{1/2} \} ,$$

$$m_2^{(0)} = 0 ,\qquad\qquad\qquad\qquad\qquad\text{(A1)}$$

$$d_1^{(0)} = \frac{d_1^0}{1+m_1^{(0)}} ,$$

$$d_2^{(0)} = \frac{d_2^0}{1+\beta m_1^{(0)}}$$

and the solution obtained by a permutation of the indices 1 and 2.

The solution corresponding to $m_2^{(0)} = 0$ is acceptable only when $m_1^{(0)} > 0$, this occurs when the laser is above the first threshold: $d_1^0 > 1/1 + \alpha\beta$. The solution $m_1^{(0)} = 0$ is acceptable when $d_2^0 > 1/1 + \alpha\beta$.

The variation of m_1 with the pump parameter is not rigorously linear, but with the typical experimental values of the parameters, between the two thresholds, the laser intensity in mode 1 may be approximated as

$$m_1^{(0)} = \frac{1+\alpha\beta}{1+\alpha\beta^2}(A-1) + O((A-1)^2) . \qquad \text{(A2)}$$

(3) The two-mode solution

$$m_1^{(0)} = \frac{1}{1-\beta^2}[(1+\beta)(d_1^0 - \beta d_2^0) - (1-\beta)] ,$$

$$m_2^0 = \frac{1}{1-\beta^2}[(1+\beta)(d_2^0 - \beta d_1^0) - (1-\beta)] , \qquad \text{(A3)}$$

$$d_i^{(0)} = \frac{1}{1+\beta} .$$

This solution is acceptable only if $m_2^{(0)} > 0$. This occurs only when $\alpha > \beta$ and the laser is above the second threshold $d_1^0 > (1-\beta)/(1+\beta)(\alpha-\beta)$.

The linear stability analysis for each steady state leads to the study of the eigenvalues of a 4×4 matrix. The stability of the solutions is determined using the Routh-Hurwitz criterion applied to the characteristic equation of each matrix. The determination of the eigenvalues in the case of the monomode and two-mode solutions leads to the resolution of third- and fourth-order equations respectively. Fortunately in our OFL γ amounts to be about 10^{-3}. This allows expansion of these roots in a power series of $\gamma^{1/2}$ which will be limited to the second order. This approximation is justified when the laser is well above threshold. The results of the linear stability analysis are as follows.

(1) Trivial solution: The eigenvalues are

$$\lambda_{1,2} = -\gamma, \lambda_3 = -[1-(d_1^0 + \beta d_2^0)] ,$$
$$\lambda_4 = -[1-(d_2^0 + \beta d_1^0)] . \qquad\qquad \text{(A4)}$$

The trivial solution is therefore stable only if the laser is below the first threshold ($d_1^0 < 1/1 + \alpha\beta$).

(2) Single-mode solution: In the case $\alpha < 1$, the solution corresponding to $m_1^{(0)} = 0$ and $m_2^{(0)} > 0$ is always unstable. For the other solution ($m_2^{(0)} = 0; m_1^0 > 0$), the first eigenvalue is

$$\lambda_1 = d_2^{(0)} + \beta d_1^{(0)} - 1 . \qquad\qquad \text{(A5)}$$

It is negative only if

$$d_1^0 < \frac{(1-\beta)}{(1+\beta)(\alpha-\beta)} ,$$

i.e., when the laser is below the second threshold. The other eigenvalues are solutions of

$$\lambda^3 + \gamma \left[\frac{d_1^0}{d_1^{(0)}} + \frac{d_2^0}{d_2^{(0)}} \right] \lambda^2 + \left[\gamma^2 \frac{d_1^0 d_2^0}{d_1^{(0)} d_2^{(0)}} + \gamma m_1^{(0)} (d_1^{(0)} + \beta^2 d_2^{(0)}) \right] \lambda + \gamma^2 m_1^{(0)} \left[\frac{d_1^{(0)}}{d_2^{(0)}} d_2^0 + \beta^2 \frac{d_1^{(0)}}{d_2^{(0)}} d_1^0 \right] = 0 \ . \tag{A6}$$

All these solutions have a negative real part only when the laser is above the first threshold. They can be expanded in power series of $\gamma^{1/2}$

$$\lambda_2 = - \frac{\dfrac{d_1^{(0)}}{d_2^{(0)}} d_2^0 + \dfrac{d_2^{(0)}}{d_1^{(0)}} d_1^0}{d_1^{(0)} + \beta^2 d_2^{(0)}} \gamma + O[(\gamma^{1/2})^3] \tag{A7}$$

and

$$\lambda_{3\pm} = \Gamma \pm i\omega \tag{A8}$$

with

$$\Gamma = - \left| \frac{\gamma}{2} \right| \frac{d_1^0 + \beta^2 d_2^0}{d_1^{(0)} + \beta^2 d_2^{(0)}} + O[(\gamma^{1/2})^4] \ .$$

and $\omega = \sqrt{A-1} + O[(\gamma^{1/2})^3]$. This linear dependence of ω^2 coincides with the predictions of the model of the two-level monomode class-B laser [13] and is observed experimentally. However, the value of Γ derived here does not agree with the experimental observations because between the two thresholds, it is strongly modified by spontaneous emission.

(2) Two-mode solution: The eigenvalues of the system are the solutions of

$$\lambda^4 + \gamma(1+\beta)(d_1^0 + d_2^0)\lambda^3 + \left[\gamma^2 d_1^0 d_2^0 (1+\beta^2) + \frac{\gamma}{1+\beta}(1+\beta^2)(m_1^{(0)} + m_2^{(0)}) \right] \lambda^2$$

$$+ \gamma^2 [m_1^{(0)}(d_2^0 + \beta^2 d_1^0) + m_2^{(0)}(d_1^0 + \beta^2 d_2^0)]\lambda + \gamma^2 m_1^{(0)} m_2^{(0)}(1-\beta^2) = 0 \ . \tag{A9}$$

All the solutions have a negative real part only when the laser is above the second threshold. These eigenvalues can be written

$$\lambda_{1,2\pm} = \Gamma_{1,2} \pm i\omega_{1,2} \tag{A10}$$

with

$$\Gamma_{1,2} = -\tfrac{1}{4}(1+\beta) \left[d_1^0 + d_2^0 \pm \frac{(1+\beta)(d_1^0 - d_2^0)^2}{\left[(m_1^{(0)} - m_2^{(0)})^2 + \dfrac{16\beta^2 m_1^{(0)} m_2^{(0)}}{(1+\beta)^2} \right]^{1/2}} \right] \gamma + O(\gamma^{1/2})^4]$$

and

$$\omega_{1,2} = \frac{1}{\sqrt{2}} \left[\frac{1+\beta^2}{1+\beta}(m_1^{(0)} + m_2^{(0)}) \pm \left[(m_1^{(0)} - m_2^{(0)})^2 + \frac{16\beta^2 m_1^{(0)} m_2^{(0)}}{(1+\beta)^2} \right]^{1/2} \right]^{1/2} \sqrt{\gamma} + O[(\gamma^{1/2})^3] \ .$$

$\Gamma_{1,2}$ depends on spontaneous emission at the first order in a, therefore the expressions of $\Gamma_{1,2}$ correspond only to the asymptotic behavior of the damping coefficients in the limit $A \gg 1$. However because spontaneous emission does not modify $\omega_{1,2}$ at the first order, the values of the frequencies determined here agree well with the experimental findings. In the case of a small asymmetry, namely when $\alpha = 0.85 - 1$ as it is the case in our experiments and when the laser is sufficiently above the second threshold, the high and low frequencies ω_1^2 and ω_2^2 depend almost linearly on the pump parameter and follow the scaling laws derived in Refs. [2,25]. They correspond to the experimentally measured quantities ω_r^2 and ω_{LF}^2.

[1] K. Otsuka, Phys. Rev. Lett. **67**, 1090 (1991). In winner-takes-all dynamics, the laser intensity switches from one mode to another, but at each time the intensity is concentrated on only one mode.

[2] K. Otsuka, P. Mandel, S. Bielawski, D. Derozier, and P. Glorieux, Phys. Rev. A **46**, 1692 (1992).

[3] D. Derozier, S. Bielawski, and P. Glorieux, Opt. Commun. **83**, 97 (1991).

[4] H. De Lang, Philips Res. Rep. Suppl. **8** (1967); D. Lenstra, Phys. Rep. **59**, 299 (1980).

[5] A. P. Voitovich, L. P. Svirina, and V. N. Severikov, Opt. Commun. **80**, 435 (1991) and references therein; A. Le Floch, G. Ropars, J. M. Lenormand, and R. Le Naour, Phys. Rev. Lett. **52**, 918 (1984); A. Le Floch, G. Ropars and R. Le Naour, Europhys. Lett. **3**, 695 (1987); W. Culshaw and J. Kannelaud, Phys. Rev. **145**, 257 (1966); **156**, 308 (1967).

[6] S. R. Chinin and H. Y. P. Hong, Opt. Commun. **15**, 345 (1975); J. Nakano, K. Otsuka, and T. Yamada, J. Appl. Phys. **47**, 2749 (1976); K. Otsuka, K. Kubodera, and J. Nakano, IEEE J. Quantum Electron. **QE-13**, 398 (1977).

[7] D. W. Hall, R. A. Haas, W. F. Krupke, and M. J. Weber, IEEE J. Quantum Electron. **QE-19**, 1704 (1983).

[8] M. Arjona, R. Corbalan, F. Laguarta, R. Pujol, and R. Vilaseca, Phys. Rev. A **41**, 6559 (1990).

[9] D. W. Phillion, D. J. Kuizenga, and A. E. Siegman, J. Chem. Phys. **61**, 3828 (1974); K. C. Reyzer and L. W. Casperson, J. Appl. Phys. **51**, 6075 (1980); **51**, 6083 (1980); L. W. Casperson, W. J. Sandle, A. C. Wilson, D. M. Warrington, and R. J. Ballagh, *ibid.* **69**, 8005 (1991).

[10] M. J. F. Digonnet and C. J. Gaeta, Appl. Opt. **24**, 333 (1985).

[11] L. A. Lugiato, F. Prati, L. M. Narducci, P. Ru, J. R. Tredicce, and D. K. Bandy, Phys. Rev. A **37**, 3847 (1988).

[12] M. Le Flohic, P.-L. Francois, J.-Y. Allain, F. Sanchez, and G. M. Stephan, IEEE J. Quantum Electron. **QE-27**, 1910 (1991); S. A. Zenchenko, S. V. Leshkevich, A. I. Portnyagin, S. P. Puchek, and A. E. Filippov, Kvant. Elektron. (Moscow) **17**, 841 (1990) [Sov. J. Quantum Electron. **20**, 760 (1990)].

[13] O. Svelto, *Principles of Lasers,* 1st ed. (Plenum, New York, 1976).

[14] D. T. Cassidy, J. Opt. Soc. Am. **B8**, 747 (1991); G. P. Agrawal, Appl. Phys. Lett. **49**, 1013 (1986); Y. C. Shen, H.

G. Winful, and J. M. Liu, *ibid.* **47**, 208 (1985).

[15] D. C. Hanna, R. G. Smart, R. J. Suni, A. I. Ferguson, and M. W. Phillips, Opt. Commun. **68**, 128 (1988); M. W. Phillips, H. Gong, A. I. Ferguson, and D. C. Hanna, *ibid.* **61**, 215 (1987).

[16] D. Dangoisse, P. Glorieux, and D. Hennequin, Phys. Rev. A **36**, 4775 (1987); F. T. Arecchi, R. Meucci, G. P. Puccioni, and J. R. Tredicce, Phys. Rev. Lett. **49**, 1217 (1982); T. Midavaine, D. Dangoisse, and P. Glorieux, *ibid.* **55**, 1989 (1985); J. Legrand, C. Lepers, and P. Glorieux, Phys. Rev. A **43**, 2573 (1991).

[17] K. Wiesenfeld, C. Bracikowski, G. James, and R. Roy, Phys. Rev. Lett. **65**, 1749 (1990); G. E. James, E. M. Harell II, and R. Roy, Phys. Rev. A **41**, 2778 (1990); C. Bracikowski and R. Roy, *ibid.* **43**, 6455 (1991).

[18] P. Bergé, Y. Pomeau, and Ch. Vidal, *Order Within Chaos* (Wiley, New York, 1984).

[19] R. S. Quimby, Appl. Opt. **29**, 1268 (1990).

[20] R. I. Laming, S. B. Poole, and E. J. Tarbox, Opt. Lett. **13**, 1084 (1988).

[21] T. Baer, J. Opt. Soc. Am. **B3**, 1175 (1986); B. A. Niyazov and F. R. Sultanova, Opt. Commun. **80**, 397 (1991).

[22] C. L. Tang, H. Statz, and G. de Mars, J. Appl. Phys. **34**, 2289 (1963); E. A. Victorov, I. B. Vitrischak, G. E. Novikov, O. A. Orlov, A. A. Mak, V. A. Sokoilov, V. I. Ustyugov, and M. M. Khaleev, in *Proceedings on Nonlinear Dynamics of Optical Systems,* edited by N. B. Abraham *et al.* (Optical Society of America, Washington, DC, 1991), Vol. 7, p. 410.

[23] P. Manneville, *Dissipative Structures and Weak Turbulence* (Academic, New York, 1990).

[24] W. L. Barnes, P. P. Markel, and J. E. Townsend, Opt. Commun. **82**, 282 (1991).
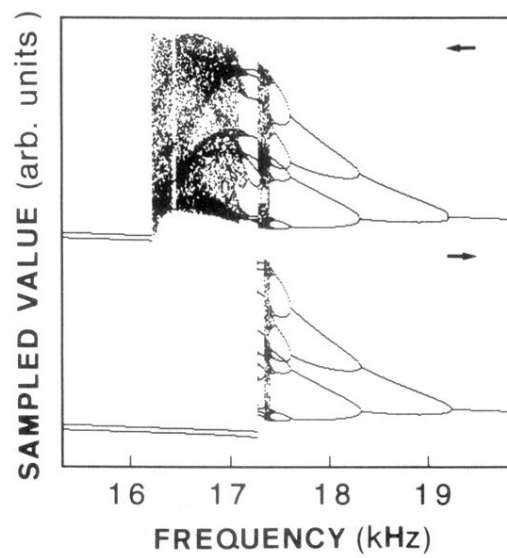
[25] P. Mandel, M. Georgiou, and K. Otsuka (unpublished).

FIG. 10. Calculated bifurcation diagrams corresponding to the experimental results of Fig. 6 with $1/(\tau_c \tau_f) = 8.75 \times 10^9$ s^{-2}.
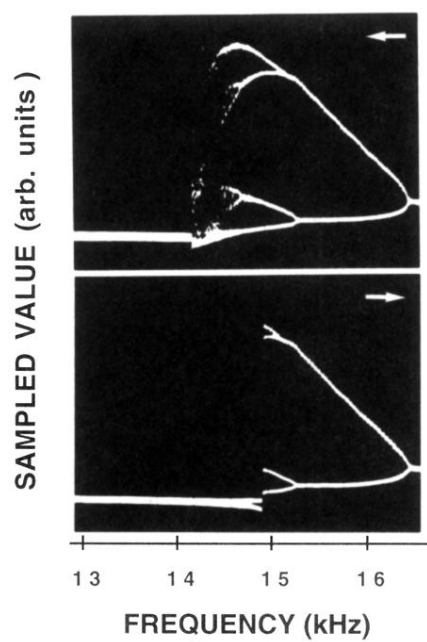
FIG. 6. Bifurcation diagram of the OFL operating at 1.08 μm. The control parameter is the frequency of the pump modulation. The upper diagram corresponds to a decreasing sweep and the lower diagram to an increasing sweep.
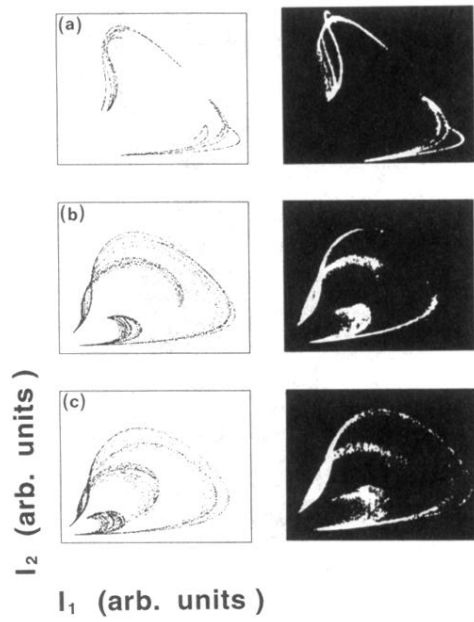
FIG. 7. Poincaré sections in chaotic regimes corresponding to different points of the inverse cascade. (a) $C2$; (b) and (c) fully chaotic regimes just after the $2C$-C transition and just before the boundary crisis. The right (left) column reports the experimental (numerical) results.